

Robin Guillaume-Castel<sup>1</sup> and Benoit Meyssignac<sup>1</sup>

<sup>1</sup>Affiliation not available

April 25, 2024

## Abstract

The pattern of surface warming plays a significant role in the Earth's response to radiative forcing as it influences climate feedbacks. Distinct patterns of surface warming lead to divergent equilibrium and transient responses to identical forcing, emphasizing the need to analyse this pattern effect. While existing studies have primarily focused on assessing the influence of surface warming patterns on long-term warming (equilibrium climate sensitivity, committed warming), their role on the transient global warming remains poorly understood. Here, we introduce a novel analytical method to quantify the importance of evolving surface warming patterns on transient global warming. Our approach involves explicitly separating the radiative response caused by the global surface warming from the additional response induced by changing surface temperature patterns in the global energy budget. Using this new energy balance model, we assess the relative contribution of the radiative response induced by changing surface temperature patterns to global warming in idealized forcing experiments (1pctCO2) from 12 CMIP6 models. We show that the pattern effect consistently dampens global warming in 11 out of 12 model at decadal time scales. Specifically, we quantify that the transient climate response is reduced on average by 11% because of changing warming patterns. Our study demonstrates that distinct models exhibit significantly divergent transient global warming solely due to variations in the pattern effect. Overall, our results highlight the importance of changing warming patterns, through the pattern effect, in influencing decadal-scale transient warming. These findings support recent suggestions to incorporate warming pattern uncertainties in future climate projections.

## Introduction

Understanding what causes changes in global mean surface temperature (GMST) is one of the most critical aspects of climate change science as GMST changes play a key role in the Earth energy budget. GMST is also a key driver of regional climate change and associated impact drivers. Indeed, the pattern of many variables like surface temperature, ocean heat content, sea level change, precipitation extremes and others, scale with GMST making GMST a relevant index of future local changes (Santer et al., 1990; Mitchell, 2003; Perrette et al., 2013; Grose et al., 2017).

GMST changes are governed by the Earth's energy budget both at the top of the atmosphere (TOA) and at the surface (Archer & Pierrehumbert, 2011). In recent decades, growing evidence has highlighted how the response of the top of the atmosphere energy budget to increasing radiative forcing is intricately linked to surface warming patterns through their radiative effect at the TOA (Andrews et al., 2015; Armour et al., 2013), a phenomenon usually referred to as the "pattern effect" (Stevens et al., 2016; IPCC, 2021). In particular, the tropical Pacific temperature gradient between the Indo-Pacific warm-pool to the West and the cold tongue to the East has been shown to affect the Pacific Walker circulation, a process associated with changes in low cloud amount in subsidence areas in the Eastern Pacific. As a result, the cloud radiative effect is changed leading to substantial changes in the TOA energy budget (Andrews & Webb, 2018; Ceppi & Gregory, 2017; Schiro et al., 2022; Zhou et al., 2017).

Long term warming, such as the equilibrium climate sensitivity (ECS), or the committed warming, is significantly affected by these warming patterns (Andrews et al., 2018; Andrews et al., 2022; Armour, 2017; Dong

et al., 2021; Marvel et al., 2018; Sherwood et al., 2020; Zhou et al., 2021). However, the implications of these patterns on the transient trajectory of global warming are still poorly understood and not well quantified (Andrews et al., 2022; Dong et al., 2022; Frey et al., 2017; Zhou et al., 2021). Recent studies (Alessi & Rugenstein, 2023) have highlighted how the changing warming patterns may contribute to uncertainties in climate projections, emphasizing the critical need for further investigating and quantifying their role during transient warming periods.

This paper introduces a novel approach using a recently developed multivariable energy balance model (Meyssignac et al., 2023) to quantify the pattern effect’s influence on transient warming. By explicitly separating the contributions of global surface warming from the contribution of changing warming patterns to the Earth’s radiative response, we provide a relevant framework for quantifying and interpreting the impact of the pattern effect on transient global warming. Section 2 outlines the development of the multivariable energy balance model and its application in assessing the GMST change attributable to the pattern effect. Section 3 describes the data and methodology employed to evaluate the pattern effect and its impact on global warming in climate model simulations. In Section 4, we detail our findings, followed by a discussion in Section 5 that explores the implications of our results and the limitations of our approach. The paper concludes with a summary of our key insights in Section 6.

## Analytical decomposition of the radiative response of the Earth

We assume that the pre-industrial climate is in a dynamical steady state. From there, the radiative forcing change induced by increasing atmospheric concentration of carbon dioxide  $F$  causes a global energy imbalance  $N$ . In response to this imbalance, the surface temperature of the Earth changes, gradually increasing the radiative response of the Earth,  $R$ , to compensate for the imbalance induced by the increasing atmospheric concentration of carbon dioxide. The Earth energy budget reads:

$$N(t) = F(t) + R(t)$$

(1)

A common approach is to consider that the radiative response change  $R$  only depends on the GMST anomaly through a multiplicative constant  $\lambda$ , usually called the climate feedback parameter (Budyko, 1969; Sellers, 1969; North & Kim, 2017). The pattern effect has often been interpreted as a time-dependant climate feedback parameter  $\lambda(t)$  (Armour et al., 2013; Dong et al., 2019; Wills et al., 2021; Meyssignac et al., 2023). This approach has however shown limits and lead to inconsistencies in the global energy budget (Meyssignac et al., 2023). Our approach is different and consists in explicitly separating the contribution of the GMST and of changing warming patterns to the radiative response beforehand, to account for the apparent time variations in the climate feedback parameter.

The key hypothesis is that the radiative response of the Earth depends on the GMST change  $\bar{T}(t)$  but also on changes in the pattern of surface warming, noted  $T'_x(t)$ , that we define as the distance of local surface warming to global mean surface warming. By explicitly separating these two dependencies, the change in radiative response  $R$ , which follows the increased radiative forcing  $F$ , can be written using a first order Taylor expansion with regard to these different variables (Zhang et al., 2023; Bloch-Johnson et al., 2024; Meyssignac et al., 2023):

$$R(t) = \frac{\partial R}{\partial \bar{T}} \bar{T}(t) + \sum_x \frac{\partial R}{\partial T'_x} T'_x(t)$$

(2)

where  $x$  stands for the locations on the globe. Here, the radiative response is separated into two different terms. The first term corresponds to the radiative response to changes in GMST. The value of  $\frac{\partial R}{\partial T}$  corresponds to the magnitude of the net climate feedback if the warming was uniform. We note this term  $\lambda_u$ , corresponding to a uniform warming climate feedback parameter. The second term corresponds to the radiative response to changes in the surface temperature patterns with no changes in the GMST. In other words, this term represents the pattern effect. In this paper, the term *pattern effect* designates this second term, and we note it  $P$ . For simplicity,  $\frac{\partial R}{\partial T_x}$  is noted  $\eta_x$  for a given  $x$  such that  $P = \sum_x \eta_x T'_x(t)$ . This multi-variable approach is, in essence, similar to other studies where the pattern effect is represented by an external variable in the global energy budget (Ceppi & Gregory, 2019; Fueglistaler, 2019).

Incorporating the radiative response decomposition in the global Earth energy budget (Equation 1) leads to:

$$N(t) = F(t) + \lambda_u \bar{T}(t) + P(t)$$

(3)

To determine the influence of the pattern effect on the GMST change, we use the following simple two-layer diffusion model for ocean heat uptake (Dickinson, 1981; Gregory, 2000; Raper et al., 2002; Held et al., 2010; Geoffroy et al., 2013; North & Kim, 2017; Rohrschneider et al., 2019):

$$\begin{cases} C \frac{d\bar{T}}{dt} = F(t) + \lambda_u \bar{T}(t) + P(t) - \gamma(\bar{T} - \bar{T}_0) \\ C_0 \frac{d\bar{T}_0}{dt} = \gamma(\bar{T} - \bar{T}_0) \end{cases}$$

(4)

where  $C$  and  $C_0$  are the heat capacities of the surface layer and of the deep ocean layer respectively,  $\gamma$  is the diffusion heat exchange coefficient between the two layers, and  $\bar{T}_0$  is the temperature change of the deep ocean layer. By construction, the variable  $P$  represents higher moments of the surface temperature distribution than  $\bar{T}$ , which means  $P$  can be considered mostly independent from  $\bar{T}$ .

In equation 4, the pattern effect acts as a pseudo-forcing (Zhou et al., 2021), which contributes to GMST change the same way that the radiative forcing does. As a consequence, the surface GMST change can be written as the sum of two contributions: the GMST response to the radiative forcing that we note  $\bar{T}_F$ , and the GMST response to the pattern effect that we note  $\bar{T}_P$ . Similarly, the deep ocean temperature can also be written as the sum of two contributions  $\bar{T}_{0F}$  and  $\bar{T}_{0P}$ . The 2-layer energy budget now reads:

{

$$\begin{aligned}
 \bar{T}(t) &= \bar{T}_F(t) + \bar{T}_P(t) \\
 \bar{T}_0(t) &= \bar{T}_{0F}(t) + \bar{T}_{0P}(t) \\
 C \frac{d\bar{T}_F}{dt} - \lambda_u \bar{T}_F(t) + \gamma(\bar{T}_F - \bar{T}_{0F}) &= F(t) \\
 C_0 \frac{d\bar{T}_{0F}}{dt} - \gamma(\bar{T}_F - \bar{T}_{0F}) &= 0 \\
 C \frac{d\bar{T}_P}{dt} - \lambda_u \bar{T}_P(t) + \gamma(\bar{T}_P - \bar{T}_{0P}) &= P(t) \\
 C_0 \frac{d\bar{T}_{0P}}{dt} - \gamma(\bar{T}_P - \bar{T}_{0P}) &= 0
 \end{aligned}
 \tag{5}$$

Solving Equation 5 (following the same approach as (Geoffroy et al., 2013; Rohrschneider et al., 2019)) yields an analytical expression of the time changes in the GMST response to the radiative forcing and of the GMST response to the pattern effect. They read

$$\begin{aligned}
 &\{ \\
 \bar{T}_F(t) &= \frac{1}{C(\psi_s + \psi_f)} \left( \psi_f \int_0^t F(s) e^{-\frac{t-s}{\tau_f}} ds + \psi_s \int_0^t F(s) e^{-\frac{t-s}{\tau_s}} ds \right) \\
 \bar{T}_P(t) &= \frac{1}{C(\psi_s + \psi_f)} \left( \psi_f \int_0^t P(s) e^{-\frac{t-s}{\tau_f}} ds + \psi_s \int_0^t P(s) e^{-\frac{t-s}{\tau_s}} ds \right)
 \end{aligned}
 \tag{6}$$

Where  $\tau_s$  and  $\tau_f$  are slow and fast characteristic times respectively, and  $\psi_f$  and  $\psi_s$  are mode parameters (see Appendix and (Geoffroy et al., 2013; Rohrschneider et al., 2019) for more details).

Equation 6 suggests the GMST response to the pattern effect has the same temporal structure as the response to the forcing. They both show two characteristic timescales associated to the atmospheric and surface feedback strength (represented by  $\lambda_u$ ) and to the vertical heat transport in the ocean (represented by the parameters  $C$ ,  $C_0$  and  $\gamma$ ). The first timescale corresponds to an interannual to decadal response ( $\tau_s \sim 1 - 3$  years in climate models), while the second timescale represents the multidecadal to centennial response ( $\tau_f \sim 100$  years in climate models, (Smith et al., 2021)).

## Data and methods

In this section, we quantify each term of the multivariate energy budget (Equation 3) in 1pctCO2 simulations from different climate models. We separately compute the radiative response induced by a uniform warming, the pattern effect and the radiative forcing. Using these estimates, we validate the multi-variable energy balance model introduced in Section by checking that the global energy budget is closed in climate model simulations. We then use equation 6 to quantify the global mean surface temperature change induced by the pattern effect in 1pctCO2 simulations ran with climate model.

Coupled CMIP6 models	
Model	Coupled model reference
BCC-CSM2-MR	(Wu et al., 2019)
CESM2	(Danabasoglu et al., 2020)
CNRM-CM6-1	(Voldoire et al., 2019)
CanESM5	(Swart et al., 2019)
E3SM-1-0	(E3SM Project, 2018)
GFDL-CM4	(Dunne et al., 2020)
GISS-E2-1-G	(Kelley et al., 2020)
HadGEM3-GC31-LL	(Williams et al., 2018)
IPSL-CM6A-LR	(Boucher et al., 2020)
MIROC6	(Tatebe et al., 2019)
MRI-ESM2-0	(Yukimoto et al., 2019)
NorESM2-LM	(Seland et al., 2020)
Atmospheric model	Model reference / Green's functions reference
CAM4	(Neale et al., 2013) / (Dong et al., 2019)
CAM5	(Neale et al., 2010) / (Zhou et al., 2017)
GFDL-CM4	(Zhao et al., 2018) / (Zhang et al., 2023)

Table 1: Coupled models and atmospheric models used in this study.

## Data used in this study

To evaluate the transient warming in response to increasing CO<sub>2</sub> concentrations, we choose to approach the problem using idealized simulations from the latest generation of coupled climate model: CMIP6 (Eyring et al., 2016). The 1pctCO<sub>2</sub> experiment allows to simulate transient warming similar to what has been experienced in the 20<sup>th</sup> century, and what is expected to happen in the 21<sup>st</sup> century. In these simulations, carbon dioxide concentrations are increased at a rate of 1% per year from the pre-industrial concentration, leading to a doubling in CO<sub>2</sub> concentration after 70 year and a quadrupling after 140 years. This experiment is notably used to quantify a commonly used climate metric that is representative of transient warming: the Transient Climate Response (IPCC, 2021). The TCR is the GMST change reached after 70 years of the 1pctCO<sub>2</sub> experiment and is usually considered as representative of warming in the next century (Grose et al., 2018). In this paper we study the influence of the pattern effect on the time-dependant transient GMST change, but also on the TCR.

To determine  $\lambda_u$  our analysis requires models to be run with uniform warming experiments. Such experiments (notably amip-p4K, amip-m4K and piSST-pxK) are part of the Cloud Feedback Model Intercomparison Project (Webb et al., 2017). Overall 13 models were run with amip-p4K experiments, nine with amip-m4K and four with piSST-pxK. Out of the 13 models, only one (TaiESM1) was not usable because of missing data on ESGF, where CMIP data are stored.

To compute the pattern effect, we use Green's functions (GF), which are extensively detailed in (Bloch-Johnson et al., 2024). The GF are based on hundreds of climate model simulations which are combined to provide an estimate of the radiative response to a localized anomaly of sea surface temperature. Ideally, we should use each of the individual GF of all 12 CFMIP models. However, at the moment, only three GF are readily available online from three different atmospheric models (CAM4 (Dong et al., 2019), CAM5 (Zhou et al., 2017) and GFDL-AM4 (Zhang et al., 2023)). To conduct a multimodel analysis, we use all 12 CFMIP models combined with the three GF. We show later that the results are consistent regardless of the GF used. The models used and their corresponding references are presented in Table 1.

## Quantifying the radiative response induced by uniform warming

In our framework, the uniform warming climate feedback parameter,  $\lambda_u$ , is assumed to be an AOGCM specific constant that depends on the response of the atmosphere to surface warming. To determine such quantity, we use pairs of forced atmospheric simulations with similar boundary conditions, except that an additional, spatially uniform surface temperature anomaly is prescribed in one of the two simulations (usually referred to as "Cess experiments" (Cess et al., 1990)). Within CMIP6, three such pairs exist, namely amip-p4K and amip, amip-m4K and amip, and piSST-pxK and piSST. When comparing two experiments in a given pair, both the radiative forcing and the pattern of surface temperature are identical as the simulations only differ by global mean surface temperature. Therefore, subtracting the global energy budget (Equation 3) from one experiment to another leads to:

$$N_2(t) - N_1(t) = \lambda_u (\bar{T}_2(t) - \bar{T}_1(t)) \quad (7)$$

From this equation, we deduce  $\lambda_u$  by dividing the temporal averages of both terms by the GMST difference:

$$\lambda_u = \frac{\langle N_2(t) - N_1(t) \rangle}{\langle \bar{T}_2(t) - \bar{T}_1(t) \rangle} = \frac{\langle \Delta N(t) \rangle}{\langle \Delta \bar{T}(t) \rangle} \quad (8)$$

One potential caveat of this method is that in these simulations, the additional surface temperature anomaly is only prescribed to the sea surface temperature (SST). The land surface warming is therefore free to evolve, but only as a byproduct of the SST warming, which may lead to incoherent land/sea temperature contrasts and thus to biased radiative response to uniform warming. Typically, in these experiments, the ratio of GMST increase to SST increase is less than  $1.1K/K$ , while in coupled simulations of AOGCM, it is around  $1.5K/K$  (Gregory et al., 2023; Toda et al., 2021). To correct for this potential bias, we determine the expected ratio of GMST increase to SST increase  $\alpha = \frac{\Delta \bar{T}}{\Delta SST}$  using the coupled 1pctCO2 experiments and determine  $\lambda_u$  as:

$$\lambda_u = \frac{1}{\alpha} \frac{\langle \Delta N(t) \rangle}{\langle \Delta SST(t) \rangle} \quad (9)$$

We find  $\alpha = 1.45 \pm 0.05K/K$  (uncertainties indicate one standard deviation), which is consistent with the usually considered  $1.5K/K$  (Gregory et al., 2023; Toda et al., 2021). Results obtained are summarised in Table 2. The three pairs of experiments used to determine  $\lambda_u$  are generally consistent for a given model at the level of a tenth or two of  $W m^{-2}K^{-1}$ . The value we use for  $\lambda_u$  corresponds to the mean value for all pairs available per model, which yields a multimodel mean of  $-1.14 \pm 0.16W m^{-2}K^{-1}$ .

Our values are quite different from the ones computed by (Ringer et al., 2023). Indeed, they find more negative values on average for the global mean climate feedback parameter of  $-1.4W m^{-2}K^{-1}$  for amip-p4K and  $-1.53W m^{-2}K^{-1}$  for amip-m4K. This difference of magnitude can be explained by the fact that

Model	$\Delta N / \Delta \overline{SST}$ $Wm^{-2}K^{-1}$					$\alpha$	$\lambda_u$
	piSST-pxK	amip-p4K	amip-m4K	Mean	$\sigma$	$K/K$	$Wm^{-2}K^{-1}$
BCC-CSM2-MR	-	-1.79	-1.85	-1.82	0.04	1.44	-1.26
CESM2	-1.53	-1.75	-1.77	-1.68	0.13	1.38	-1.22
CNRM-CM6-1	-1.45	-1.39	-1.65	-1.50	0.14	1.48	-1.01
CanESM5	-	-1.21	-1.18	-1.20	0.03	1.46	-0.82
E3SM-1-0	-	-1.56	-	-1.56	-	1.36	-1.14
GFDL-CM4	-	-1.82	-1.88	-1.85	0.04	1.53	-1.21
GISS-E2-1-G	-	-1.92	-	-1.92	-	1.50	-1.28
HadGEM3-GC31-LL	-1.31	-1.33	-1.35	-1.33	0.02	1.44	-0.92
IPSL-CM6A-LR	-1.34	-1.25	-1.53	-1.37	0.14	1.39	-0.99
MIROC6	-	-1.99	-	-1.99	-	1.48	-1.34
MRI-ESM2-0	-	-1.79	-1.85	-1.82	0.04	1.43	-1.27
NorESM2-LM	-	-1.80	-	-1.80	-	1.52	-1.18
Mean	-1.41	-1.63	-1.63	-1.65	0.07	1.45	-1.14
$\sigma$	0.10	0.27	0.26	0.26	0.05	0.05	0.16

Table 2: Determining  $\lambda_u$  using multiple pairs of simulations

they use equation 8 to compute the global climate feedback parameter rather than equation 9, while the GMST change  $\Delta \overline{T}$  is likely underestimated, leading to a lower denominator in the fraction, hence a more negative climate feedback parameter. Furthermore, they find that the feedbacks determined from amip-m4K are systematically more stabilizing (i.e. more negative) than diagnosed from amip-p4K. They relate this difference to different land/sea warming contrasts as shown in their Table 2. Using our method, we suppress the land/sea warming contrast difference and find more consistent amip-p4K and amip-m4K values.

The radiative response induced by uniform warming is then computed by multiplying the GMST time series from each model by the uniform warming climate feedback parameter  $\lambda_u$ .

## Quantifying the pattern effect

An increasingly more common way to quantify the influence of local surface temperature changes on the global radiative response is to use Green’s functions (Barsugli & Sardeshmukh, 2002; Dong et al., 2019; Bloch-Johnson et al., 2024; Zhou et al., 2017; Alessi & Rugenstein, 2023; Zhou et al., 2023; Zhang et al., 2023; Williams et al., 2023). These functions are determined using hundreds of forced atmospheric simulations. In each simulation, a local patch of SST change is applied on top of a reference SST background state. Green’s functions are then computed using global top of atmosphere radiation budget from all of these experiments.

The green’s functions relate the increase in global radiative response per local SST change. In our framework, this is equivalent to the increase in global radiative response per local change in pattern of SST. The pattern effect (i.e. the radiative response change due to changing warming patterns) is then computed as:

$$P(t) = \sum_x GF(x) (SST(x, t) - \overline{SST}(t)) \quad (10)$$

where  $x$  indicates locations on the global ocean,  $GF(x)$  refers to the top of atmosphere radiation budget Green’s function corresponding to the location  $x$ ,  $SST(x, t)$  is the local SST change at the location  $x$  and  $\overline{SST}$  is the global mean SST change.

Green’s functions are specific to each atmospheric model used. Ideally, we should use each model’s own Green’s functions to compute the quantity  $P(t)$ . As of today, only three Green’s functions are freely available online: two for NCAR models (CAM4, (Dong et al., 2019) and CAM5 (Zhou et al., 2017)) and one from NOAA (GFDL-AM4 (Zhang et al., 2023)). They are presented in Figure S1 in the supplementary material. As shows in Figure S1, and in the Green’s Functions Model Intercomparison Project (GFMIP, (Bloch-Johnson et al., 2024)), Green’s functions are generally consistent between models, highlighting the same key regions, notably the warm pool region in the tropical Western Pacific and the tropical Atlantic to be responsible for most of the pattern effect. Although the exact limits of the important regions and the magnitude of the Green’s functions slightly differ from one model to another, we will assume that using Green’s functions from these three models allows for a first order estimate of the pattern effect in all CMIP6 models. This hypothesis should be tested for each model’s own Green’s functions in the future, but our results are mostly not dependant on the Green’s functions used.

## Estimating the radiative forcing and closing the global energy budget

To validate the multivariable approach presented in Section , we use the global energy budget (Equation 3) along with our estimates of the radiative response to uniform warming and of the pattern effect to estimate the radiative forcing  $F$ . We then compare our results with independent estimates of the radiative forcing using two additional simulations. The results for the radiative response to uniform warming and for the pattern effect are shown in Figure 2 and discussed in Section .

In 1pctCO2 experiments, the radiative forcing is, to a very good approximation, linear with time, as  $CO_2$  forcing increases logarithmically with concentration (Myhre et al., 1998; Romps et al., 2022). Therefore, there is an AOGCM specific constant  $f$  such as:

$$F(t) = f \times t \tag{11}$$

Which leads to the following energy budget, when included in Equation 3:

$$N(t) = ft + \lambda_u \bar{T}(t) + P(t) \tag{12}$$

For each model, we determine the value of  $f$  by fitting  $N(t) - \lambda_u \bar{T}(t) - P(t)$  as a linear function in time using ordinary least squares. Figure 1 shows the linear fit alongside  $N(t) - \lambda_u \bar{T}(t) - P(t)$  for all models studied. The linear forcing approximation is a generally appropriate estimate for all models, with a maximum RMSE of  $0.5W m^{-2}$  (for NorESM2-LM). We find values of  $f$  of  $0.061 \pm 0.005W m^{-2} yr^{-1}$ , which corresponds to an equivalent  $4 \times CO_2$  forcing of  $F_{4 \times CO_2} = 8.55W m^{-2}$ . These values are detailed in Table 3.

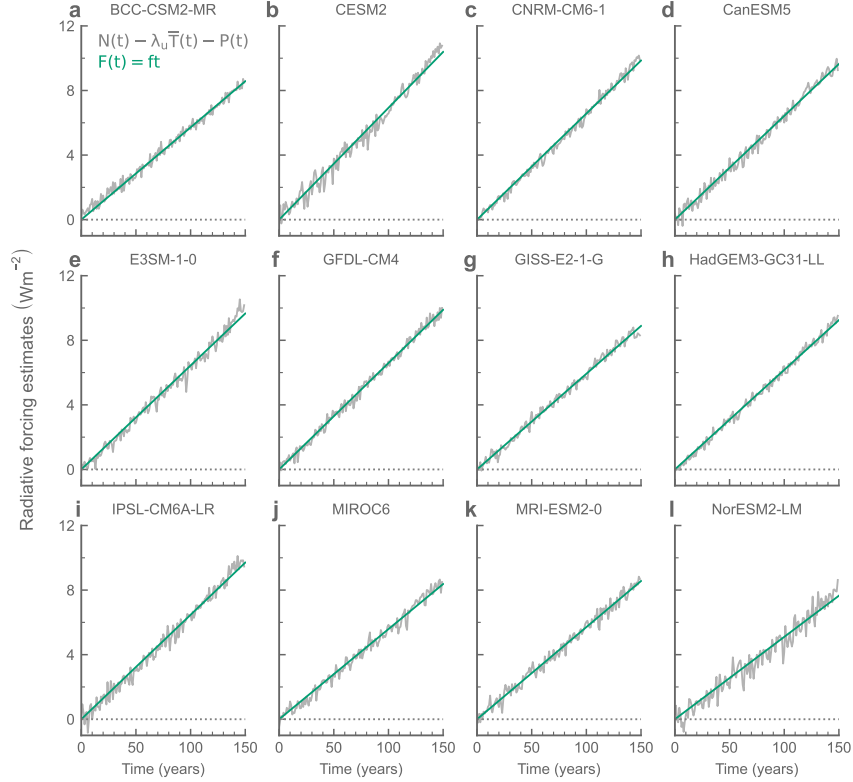


Figure 1: Linear estimates of radiative forcing using  $F(t) = ft$  (green) compared to  $N(t) - \lambda_u \bar{T}(t) - P(t)$  (grey) in 1pctCO2 experiments for all models studied. Overall, the linear approximation of the radiative forcing reproduces the temporal dynamics of the global energy budget.

We now compare our results with independent estimates of the radiative forcing. One of the commonly used method to compute radiative forcing corresponds to using fixed-SST experiments where a specific radiative forcing is applied (following (Hansen et al., 2005)). In CMIP6, these experiments are piClim-control and piClim-4xCO2, from the Radiative Forcing Model Intercomparison project (Pincus et al., 2016). In this method, two forced atmospheric simulations are run with similar boundary conditions in sea ice and sea surface temperature. The only difference between the two is that the first simulation has pre-industrial  $CO_2$  concentrations (piClim-control) and the other has 4 times this amount (piClim-4xCO2). We first estimate  $F_{4 \times CO_2} = 8.00 \pm 0.43 Wm^{-2}$ .

While the sea surface temperature is fixed, the land temperature is free to evolve, which slightly impacts the GMST, eventually biasing the radiative forcing estimates (Hansen et al., 2005; Forster et al., 2016; Smith et al., 2018). When comparing piClim-control, and piClim-4xCO2, we find a GMST difference of  $0.53 \pm 0.06 K$ , which leads to an estimated error in  $F_{4 \times CO_2}$  of  $0.60 \pm 0.11 Wm^{-2}$ . Overall, the fixed-SST method, corrected for land temperature warming leads to  $F_{4 \times CO_2} = 8.6 \pm 0.49 Wm^{-2}$ . Our estimates of  $F_{4 \times CO_2}$  are consistent with the standard fixed SST method, when corrected for land temperature warming in piClim-4xCO2 experiments (See also Figure S2 in the supplementary material) which means that the energy budget is closed and our decomposition of the energy budget in uniform response plus pattern effect response is valid at the level of a few tenth of  $Wm^{-2}$ .

Note that better estimates of the radiative forcing corrected for land warming could also be obtained directly using experiments where both the SST and the land surface temperature are prescribed (Ackerley et al., 2018). (Andrews et al., 2021) found that in one model, land warming could bias the radiative forcing

Model	$f$ ( $Wm^{-2}yr^{-1}$ )	$F_{4 \times CO_2}$ from $f$	$(Wm^{-2})$ piClim-4xCO2	+ land corrections
BCC-CSM2-MR	0.057	7.96	-	-
CESM2	0.069	9.65	8.90	9.62
CNRM-CM6-1	0.066	9.15	7.98	8.50
CanESM5	0.064	8.96	7.60	8.01
E3SM-1-0	0.064	8.97	-	-
GFDL-CM4	0.066	9.18	8.23	8.90
GISS-E2-1-G	0.059	8.26	7.96	8.76
HadGEM3-GC31-LL	0.062	8.59	8.08	8.57
IPSL-CM6A-LR	0.065	9.01	8.01	8.58
MIROC6	0.056	7.78	7.33	7.96
MRI-ESM2-0	0.057	7.95	7.66	8.19
NorESM2-LM	0.051	7.11	8.25	8.91
Average	0.061	8.55	8.00	8.60
Standard Deviation	0.005	0.74	0.43	0.49

Table 3: Radiative forcing estimates

estimates of a quadrupling of  $CO_2$  by  $1Wm^{-2}$ . Such experiments would probably provide better estimates of the radiative forcing and thus a better constraint on the validation of our approach.

Overall, using independent estimates of the uniform warming climate feedback parameter, of the pattern effect and of the radiative forcing, we reproduce the global Earth energy budget within a reasonable approximation with the multivariable energy budget (Equation 3).

## Quantifying the global mean surface temperature change induced by the pattern effect

Now that all parameters in the global energy budget (Equation 3) have been calculated, we calibrate the two-layer model (Equation 4) to determine the optimal ocean parameters  $C$ ,  $C_0$  and  $\gamma$ . For this purpose, we use a random draw of these three parameters based on the distributions of  $C$ ,  $C_0$  and  $\gamma$  from CMIP6 models, as determined by (Smith et al., 2021), following the method of (Geoffroy et al., 2013). For each CMIP6 model, we perform 10,000 numerical integrations of the two-layer model, each time with a different triplet ( $C$ ,  $C_0$  and  $\gamma$ ) from the random draw. The triplet that minimizes the distance between the reconstructed GMST through integration and the GMST output from the model is chosen for the values of the ocean parameters.

For all CMIP6 models, we find a triplet that reproduces GMST changes with a maximum RMSE of 0.16K over the 150 years of the 1pctCO2 experiment (see Figure S3 in the supplementary material). The limited RMSE confirms that with consistent values of ocean parameters, the two-layer model with the multivariable energy budget accurately reproduces the temporal evolution of the global mean surface temperature anomaly. Detailed values of  $C$ ,  $C_0$  and  $\gamma$  are provided in Table 4. As  $C$ ,  $C_0$  and  $\gamma$  have been determined from a random draw within their assessed ranges in CMIP6 (Geoffroy et al., 2013; Smith et al., 2021), they are consistent with previously published estimates.

model	$C$	$C_0$	$\gamma$	RMSE
	$Wm^{-2}K^{-1}yr$	$Wm^{-2}K^{-1}yr$	$Wm^{-2}K^{-1}$	K
BCC-CSM2-MR	6.51	152.99	0.54	0.09
CESM2	9.29	69.76	0.95	0.13
CNRM-CM6-1	9.66	63.12	0.91	0.15
CanESM5	8.43	43.97	0.93	0.11
E3SM-1-0	8.12	26.01	1.00	0.13
GFDL-CM4	6.06	59.72	1.00	0.10
GISS-E2-1-G	11.08	139.34	0.70	0.16
HadGEM3-GC31-LL	5.86	44.84	0.93	0.10
IPSL-CM6A-LR	8.90	37.49	0.84	0.15
MIROC6	10.88	117.41	0.76	0.15
MRI-ESM2-0	7.29	112.35	1.08	0.10
NorESM2-LM	9.29	69.76	0.95	0.15
Mean	8.45	78.06	0.88	0.13
sigma	1.75	42.01	0.15	0.02

Table 4: Ocean parameters for the two-layer model for each model studied. The RMSE corresponds to the error of the GMST from the integration compared with the simulated GMST.

## Results

### The pattern effect in 1pctCO2 simulations

The pattern effect, i.e. the radiative response induced by changing surface warming patterns, is shown in Figure 2 for each model studied. Compared to the radiative response to uniform warming, the pattern effect has less effect on the total radiative response of the Earth. Indeed, the pattern effect reaches mean absolute values of  $0.54 \pm 0.19 Wm^{-2}$ , which is approximately 20% of the mean absolute values of the radiative response induced by uniform warming of  $2.70 \pm 0.48 Wm^{-2}$ .

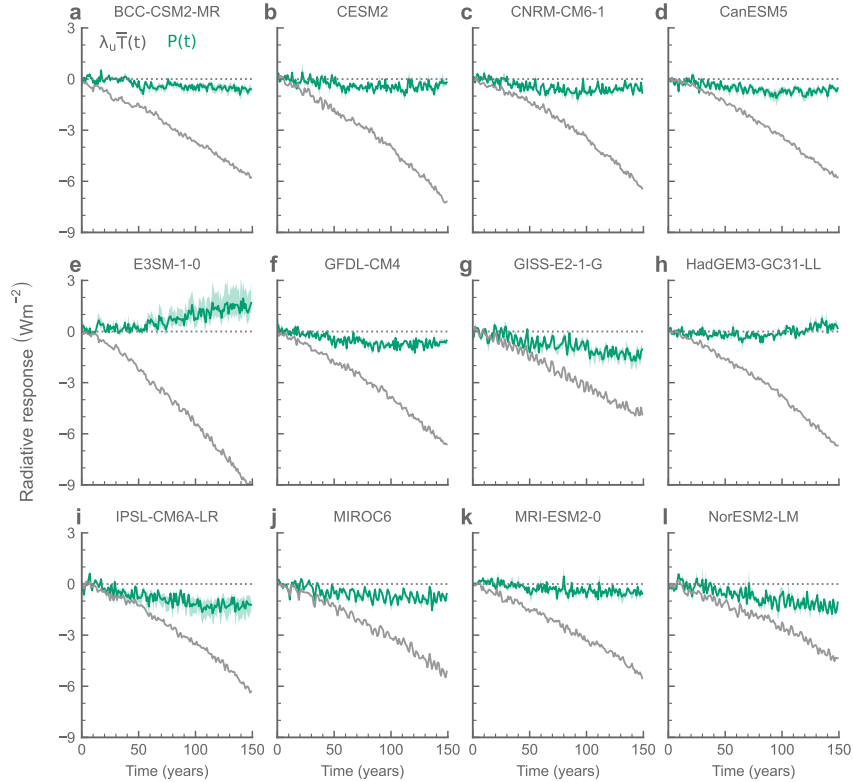


Figure 2: Annual means of the radiative response to uniform surface warming (grey) and to surface warming patterns with zero-mean change (i.e. pattern effect, green) in the 1pctCO<sub>2</sub> experiments. The green lines for the pattern effect represent the mean values obtained with the three Green's functions of CAM4, CAM5 and GFDL-CM4 models. The green shaded areas represent the minimum and maximum values reached with individual Green's functions.

In all models, the pattern effect shows significant changes at multi-decadal timescales, along with high frequency variability at annual to decadal timescales. The timeseries diagnosed for each Green's functions are shown in Figure S4 in the supplementary material.

### Multidecadal response

Our results show that changing warming patterns generally amplify the negative radiative response induced by uniform warming. In 10 out of 12 models, the pattern effect induces a negative radiative response for the entire simulation, excluding high frequency variability. During the first decades of the simulation, all models but E3SM-1-0 show a negative trend in the pattern effect. At the minimum, the pattern effect reaches a 10-year average of  $-0.97 \pm 0.34 Wm^{-2}$ . In most models, this negative trend is followed by an inflexion in the time series after 70-100 years of simulation where the pattern effect stabilizes and the trend reverses to become positive.

The pattern effect becomes positive in two models only. In this case, the pattern effect acts against the radiative response induced by uniform warming, therefore increasing the global energy imbalance. In E3SM-1-0, the pattern effect is constantly positive, with a neutral and stationary pattern effect during the first decades followed by a positive trend after 50 years of simulations. The pattern effect reaches a 10-year average of  $1.51 Wm^{-2}$  towards the end of the simulation. In HadGEM3-GC31-LL, the timeseries inflexion also yields positive values reaching a 10-year average of  $0.41 Wm^{-2}$  towards the end of the simulation.

The multidecadal change in the pattern effect is likely to be a forced response as the signal to noise ratio in 1pctCO<sub>2</sub> experiments is very high. We verified this by computing the pattern effect in three different realizations of the 1pctCO<sub>2</sub> experiment using the same climate model (CanESM5, see Figure S5 in the supplementary material). The pattern effect has the same multidecadal tendency in all three realizations and only high frequency variability is different, supporting the hypothesis of a forced signal.

To determine the regions that are responsible for this multidecadal forced signal in the pattern effect, we plot the multi-model mean and the inter-model standard deviation of the pattern of warming at the time of doubling the CO<sub>2</sub> in the atmosphere in 1pctCO<sub>2</sub> simulations (averaged over years 60 to 80, Figure 3.a-b) and convolve these maps with the mean Green's functions, computed from the three Green's Functions used in the study (Figure 3.c-d). We show that the strongest pattern values (i.e. largest deviations of local warming compared to global warming), and the strongest intermodel spread in the pattern of warming are located in high latitudes, notably in the Arctic and in the Southern Ocean, but also in the North Atlantic, and the North West Pacific. We also find that key regions where the Green's functions have the most impact on the radiative response (tropical western Pacific and tropical Atlantic) show moderate patterns and very limited inter-model spread (see Figure 3.a-b).

Despite a smaller spread in warming patterns, the tropical regions have the strongest pattern effect and generate the highest intermodel standard deviation in radiative response because of the high sensitivity of Green functions to these regions (see Figure 3.c-d). It means that differences in the pattern effect among models are governed by small differences in the pattern of warming in the key tropical regions that matter for the global energy budget. Similar maps to Figures 3.a and Figure 3.c are presented for individual models in Figures S6 and S7 respectively, in the supplementary material.

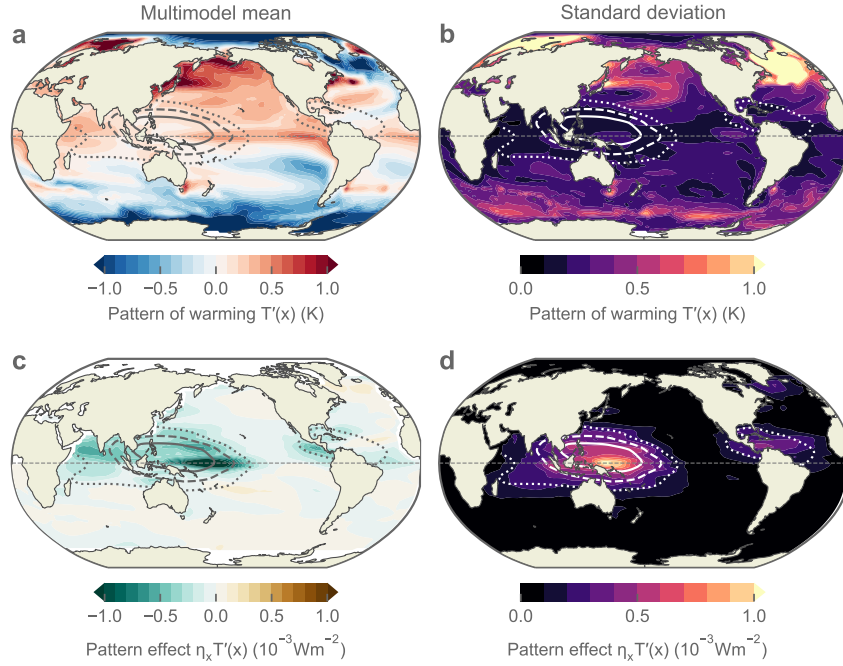


Figure 3: a. Multi model mean pattern of warming at the time of doubling carbon dioxide in 1pctCO<sub>2</sub> simulations, which correspond to local warming minus global warming, averaged over years 60-80 of the simulation. b. Inter model standard deviation of the pattern of warming. c. Multi model mean pattern effect at the time of doubling carbon dioxide in 1pctCO<sub>2</sub> simulations, obtained by convolving the pattern of warming with the mean Green's functions. d. Inter model standard deviation of the pattern effect. In all panels, the dotted, dashed and plain contour lines denote the mean Green's functions contour for 1, 2 and  $3 \times 10^{-3} W m^{-2} K^{-1}$ , respectively.

### Interannual and decadal internal variability

Along with multidecadal changes, all models show internal variability at various frequencies. The pattern effect shows high frequency internal variability (lower than 5 years, see Figure 2) that could be related to modes of internal variability that have been associated with the pattern effect such as the El Niño Southern Oscillation (Ceppi & Fueglistaler, 2021; Tsuchida et al., 2023), or the Atlantic Multidecadal Oscillation (Dessler, 2020). The Pacific Decadal Oscillation (PDO) could also explain lower frequency internal variability in the pattern effect (Loeb et al., 2018; Meyssignac et al., 2023). As Green's functions show more sensitivity to the tropical Pacific (Bloch-Johnson et al., 2024), the internal variability here is probably more associated with ENSO and the PDO than with the AMO. Note that we do not use Green's functions for sea ice as in (Bloch-Johnson et al., 2024; Dong et al., 2019), which means internal variability associated with sea ice change may be missing (Dessler, 2020).

## Influence of the pattern effect on GMST change

### Global mean temperature response to the long term forced pattern effect

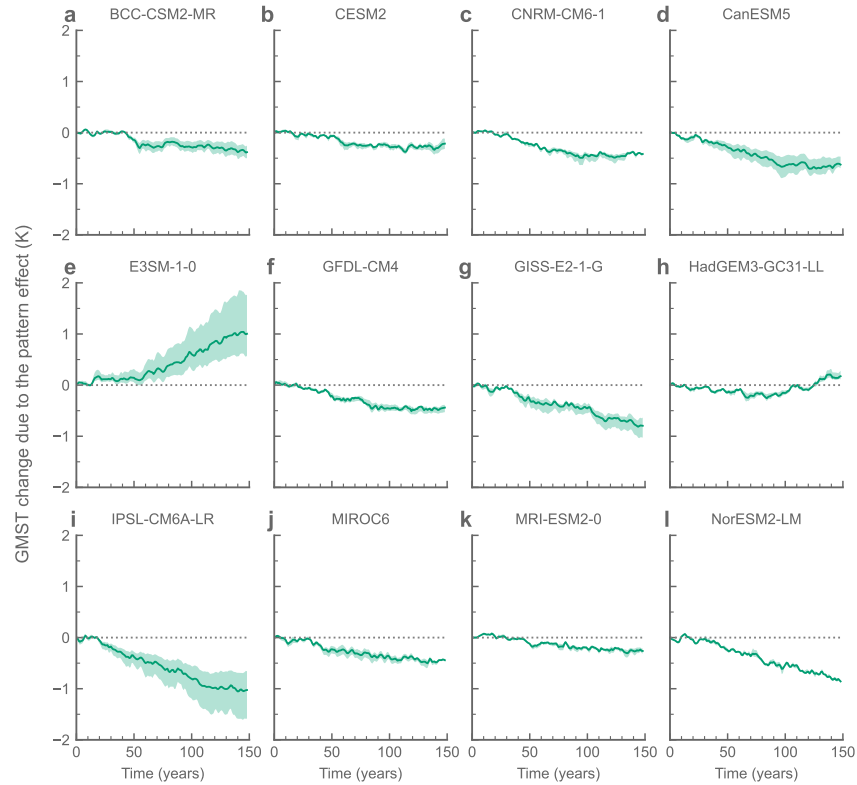


Figure 4: Global mean surface temperature change induced by changing warming patterns. The lines show the results obtained with the mean pattern effect computed from the mean of Green’s functions. The shaded areas represent the maxima and minima obtained from the different Green’s functions individually

We show the results of the influence of the pattern effect on GMST change in Figure 4. Overall, the multidecadal changes are similar to the changes in the pattern effect, but the time series are smoothed out. As the pattern effect acts as a pseudo-forcing on GMST, a negative (positive) pattern effect is equivalent to a negative (positive) forcing which induces global cooling (warming). Most models show a damping of the warming because of the pattern effect, with cooling up to 1K after 100 years of simulations. HadGEM3-GC31-LL shows slight cooling for the first 100 years and a slight warming amplification for the last 50 years. E3SM-1-0 shows intensified warming because of its simulated positive pattern effect, with warming amplified up to 1K after 150 years. The magnitude of the GMST change induced by the pattern effect can be up to 20% of the total GMST magnitude. As for the pattern effect, the spread across Green’s functions is relatively weak for most models, except for E3SM-1-0 and IPSL-CM6A-LR, where the general behaviour is similar across Green’s functions, but with different magnitudes.

As presented earlier, the Transient Climate Response (TCR) is defined as the GMST change in response to increasing  $CO_2$  concentrations at a rate of 1% per year until two times the pre-industrial concentrations are reached (IPCC, 2021). The TCR hence corresponds to year 70 in the 1pctO2 time series studied here. The TCR can be decomposed into two parts. The first one is directly related to the response of the global energy budget to the radiative forcing ( $TCR_F$ ), and the second part is the additional GMST change induced by

the pattern effect ( $TCR_P$ ), such that:

$$TCR = TCR_F + TCR_P \tag{13}$$

For each model, we quantify  $TCR$ ,  $TCR_F$  and  $TCR_P$  by taking the average  $\bar{T}$ ,  $\bar{T}_F$  and  $\bar{T}_P$  during the years 60-80 to reduce the influence of internal variability (Dong et al., 2021). The results are presented in Figure 5. We show that the TCR is consistently reduced by the pattern effect in 11 out of 12 models., with a mean reduction of 11%.

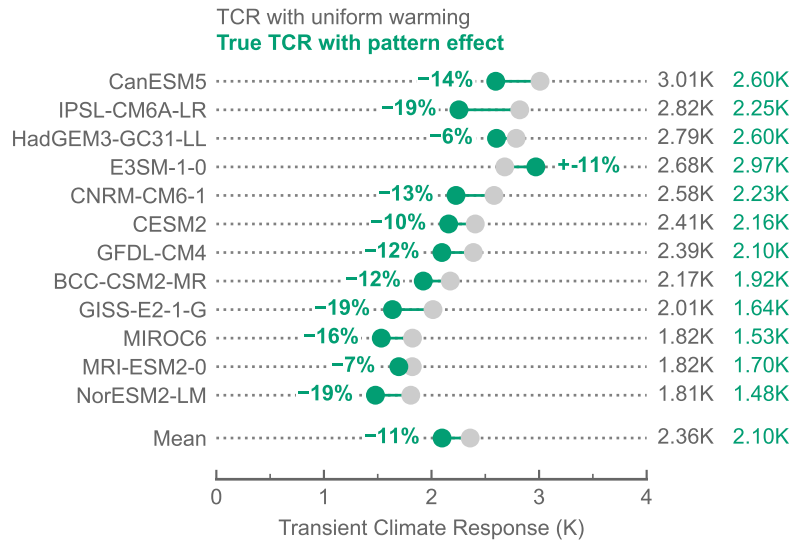


Figure 5: Contribution of the uniform response of the global energy budget (grey) and of the pattern effect (green) to the Transient Climate Response. Numbers to the right indicate the TCR in direct response to the radiative forcing, i.e. if the warming pattern had not changed (in grey) and the true TCR value in green, which also accounts for the pattern effect. Percentages show the percent of reduction or increase in GMST change due to the pattern effect compared to a uniform response of the global energy budget.

Overall, our analysis shows that the pattern effect generally reduces transient warming when responding to  $CO_2$ . Still, models show differences in the magnitude of this GMST change mediated by the pattern effect, which means that similar responses to the radiative forcing may lead to different global warming because of the pattern effect. As an example, three models studied would have a very similar TCR if the warming was uniform, but they have a different pattern effect: IPSL-CM6A-LR, HadGEM3-GC31-LL and E3SM-1-0. Their TCR standard deviation is increased from 0.07K with uniform warming to 0.36K because of the pattern effect. Our findings highlight the importance of taking the pattern effect into account when analysing decadal scale GMST change in response to radiative forcing. This supports the recent claim that the pattern effect should be considered for decadal to centennial climate projections (Alessi & Rugenstein, 2023).

### Global mean temperature response to the internal variability of the pattern effect

Internal variability has a different effect on the GMST change induced by the pattern effect than on the pattern effect itself. Indeed, when integrating the radiative response of the Earth to get the associated GMST changes, the ocean acts as a low pass filter on the radiative forcing (see Equation 5 and (Geoffroy et al., 2013)). The ocean acts the same way on the radiative response associated to the pattern effect. This means that the high frequency variability of the pattern effect is mostly filtered out during the integration and will not affect the GMST. The two-layer model in equation 5 represents this ocean filter as a second order low-pass filter, with a cutoff period given by:

$$(14) \quad \tau = -2\pi \frac{\lambda_u}{C}$$

We estimate this cutoff period to be  $47 \pm 11$  years in the models studied.

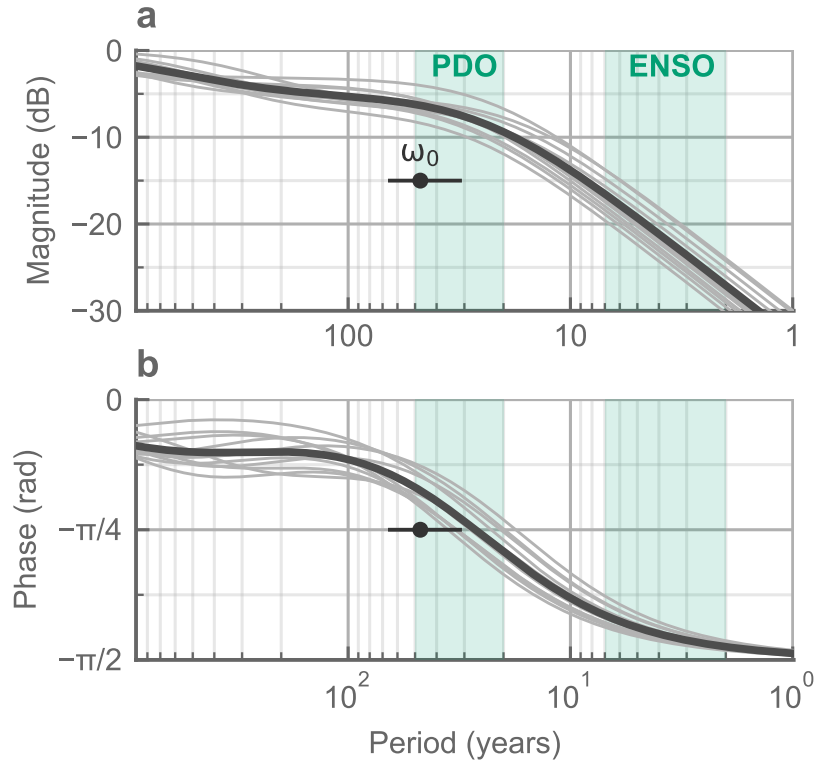


Figure 6: Bode plot for the low pass filter corresponding to the two-layer model for each model studied. In both panels, individual models are shown in light grey and the multimodel mean are shown in darker grey with thicker lines. The mean and total range of the cutoff frequencies  $\omega_0$  are displayed with a grey marker and a grey horizontal line respectively. Periods roughly corresponding to ENSO and the PDO are indicated with the green shaded areas. a. Magnitude reduction of the filter. b. Phase shift of the filter.

The bode plot of the the two-layer model of Equation 5 is presented in Figure 6. It shows the magnitude of reduction and the phase shift for each period of internal variability. High frequency variability of the pattern effect associated for example with ENSO (Ceppi & Fueglistaler, 2021) or sea ice changes (Dessler, 2020) will be strongly attenuated and will affect GMST change only marginally. However, lower frequency internal variability, such as the PDO will be hardly damped and will affect GMST change much more intensely, although with a lag of about a quarter of the period of the low frequency internal variability. This supports previous results from observations (Loeb et al., 2018; Meyssignac et al., 2023).

## Discussion

### Remaining errors in the multivariate energy balance model reconstruction

In Section , we use a multivariate energy balance model to reproduce the Earth energy imbalance as shown in Figure 1. Although it is an appropriate approximation at multidecadal time scales, there are still some slight deviations towards the last decades of the simulations. These deviations could be explained by two different causes, which are the non-logarithmic forcing of  $CO_2$ , and the feedback temperature dependence.

We assumed that the radiative forcing is logarithmically increasing with time. This approximation is a very good first order approximation, but can be limited (Gregory et al., 2015; Etminan et al., 2016). Notably (Gregory et al., 2015) showed that this approximation could lead to errors in interpreting the GMST change in 1pctCO2 experiments. Instead of using a linear approximation, they parameterize the forcing as:

$$F(t) = f_1 t + f_2 t^2 \quad (15)$$

Using ordinary least squares on the CESM2 run, which has the largest errors using equation 3, we estimate  $f_1 = 0.006 W m^{-2} yr^{-1}$  and  $f_2 = 6.5 \times 10^{-5} W m^{-2} yr^{-2}$ , which is consistent with the values found by (Gregory et al., 2015). Such estimates of the forcing slightly reduces the RMSE between the true Earth energy imbalance and the multivariate energy balance model from  $0.43 W m^{-2}$  to  $0.40 W m^{-2}$ , and produces a visually better reconstruction (see Figure S8.a in the supplementary material).

To determine Equation 2 for the multivariate radiative response, we only used the first order Taylor expansion. However, several studies (Bloch-Johnson et al., 2021; Ceppi & Gregory, 2019) suggest that models show a feedback temperature dependence that becomes significant for high GMST change. Regardless of changing patterns, this would mean that the radiative response to uniform warming is not linear but quadratic with the GMST change. With this additional quadratic dependence, the Earth energy imbalance (Equation 3) would read:

$$N(t) = F(t) + \lambda_1 \bar{T}(t) + \lambda_2 \bar{T}^2(t) + P(t) \quad (16)$$

(Bloch-Johnson et al., 2021) show that CESM2 has one of the highest feedback temperature dependence of the 14 models they studied. To test the influence of the feedback temperature dependence on our reconstruction, we use an approximate value of  $\lambda_2 = 0.04 W m^{-2} K^{-2}$ , which is within the range of (Bloch-Johnson et al., 2021). With this, the RMSE between the Earth energy imbalance and the multivariate energy balance

approximation for CESM2 goes from  $0.43Wm^{-2}$  to  $0.39Wm^{-2}$ , which is of similar magnitude as if the forcing was non logarithmic. The fit is also visually better as shown in Figure S8.c.

These two sources of error could explain the differences between the multivariable energy budget (Equation 3) and the Earth energy imbalance for the last decades of the simulation. However, determining precisely which one has the most impact here would require further investigation. To accurately quantify these two potential sources of error, one could use specific simulations to determine their individual contributions. The non-logarithmic forcing of  $CO_2$  could be determined using a piClim-1pctCO2 simulation, which would be a fixed-SST experiment, similar to piClim-4xCO2, but with gradually increasing  $CO_2$  concentrations. This would be, in essence, similar to piClim-histall experiments from RFMIP (Pincus et al., 2016). The non-logarithmic forcing would not lead to reconstruction errors with such an explicit estimate of radiative forcing. The feedback temperature dependence for uniform warming could be determined using several uniform warming experiments with various warming levels (amip-p2K, amip-p4K, amip-p6K) as in (Ceppi & Gregory, 2019). This way, the quadratic dependence of the radiative response on uniform warming could be estimated. Note that some additional non-linearities could also arise from the Green's functions (Williams et al., 2023; Bloch-Johnson et al., 2024), which would require more elaborate developments to determine the pattern effect. These potential errors have not been quantified in this study.

## Relevance for historical and future warming

In this study, we only looked at an idealized setup to study transient warming. However, key elements are missing to compare our results with historical and future warming. First, we mostly focused on the forced component, while internal variability is more important compared to the forced response in historical or future warming (Meyssignac et al., 2023; Dessler, 2020; Chao et al., 2022). Second, we only looked at the pattern effect induced by  $CO_2$  radiative forcing. However, different forcing agents can induce different pattern effects (Zhou et al., 2023; Salvi et al., 2023), and notably aerosol forcing has been identified as a key driver of warming pattern formation (Hwang et al., 2024; McMonigal, 2024; Günther et al., 2022) which is not taken into account in our idealized case.

To check the relevance of our results for historical warming simulations regarding the forced response, we compare our results with historical simulations. We compute the pattern effect time series in historical simulations using the same method as in Section and averaged the results over all ensemble members available for each model to only extract the forced response. The pattern effect time series are presented in Figure S9 in the supplementary material. Overall, we find that the forced pattern effect is also generally negative in historical simulations, which would damp global warming as in 1pctCO2 simulations. Figure 7 shows the magnitude of the pattern effect during the first 30 years of the 1pctCO2 simulations compared to the last 30 years of the historical simulations. We find that models that tend to have more negative pattern effect in 1pctCO2 simulations also have more negative pattern effect in historical simulations (with a Pearson's  $r$  value of 0.54). Although the quantification is limited, this shows that the forced pattern effect in response to  $CO_2$  increase is relevant for the forced historical response. Our results suggest that during the historical period, the pattern effect may be generally dominated by  $CO_2$  forcing. Further studied could apply our analysis to separate forcing experiments using RFMIP simulations such as piClim-GHG, piClim-aer and so on.

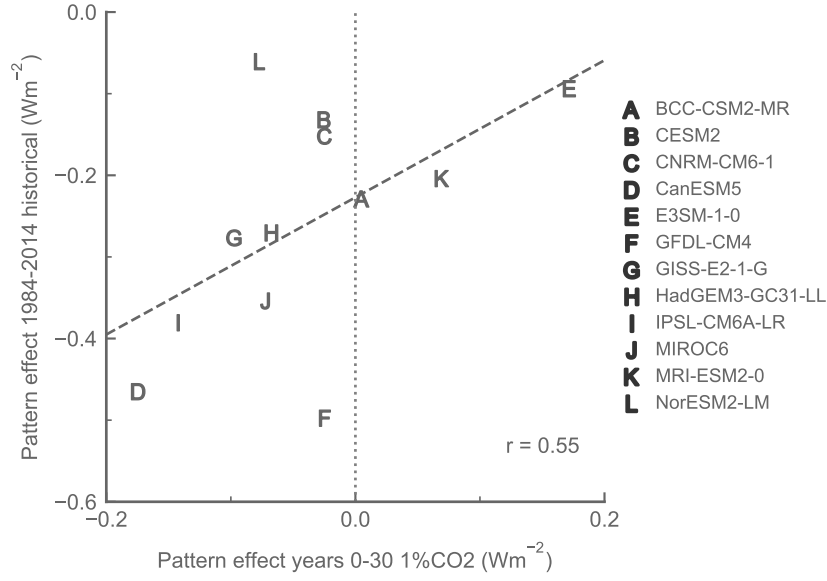


Figure 7: Comparing the pattern effect in historical simulations and in 1pctCO<sub>2</sub> simulations. The letters indicate the mean pattern effect in the first 30 years of the 1pctCO<sub>2</sub> simulation (x-axis) and the ensemble-mean pattern effect over the years 1984-2014 in historical simulations (y-axis) for each model studied. The dashed line shows the regression line between the two variables.

Figure 7 only shows the forced response comparison. Contrary to 1pctCO<sub>2</sub> runs, historical simulations are much more subject to internal variability compared to the forced signal. Our results suggest that high frequency variability such as ENSO (Ceppi & Gregory, 2019; Tsuchida et al., 2023) should not impact the GMST through their radiative response in historical simulations as it is filtered out by the low pass filter imposed by the ocean dynamics. However, internal variability associated with the PDO is likely to affect GMST in historical simulations or in the real world. Further study should investigate the influence of low frequency variability on the pattern effect (Wills et al., 2021)

Multiple studies highlight that the pattern of warming in historical simulations is different than the pattern in observed SST, which is likely due to systematic biases in climate models (Seager et al., 2022; Wills et al., 2022). Notable biases in tropical warming gradients have been associated with divergent radiative response (Fueglistaler & Silvers, 2021; Andrews et al., 2022; Armour, 2017; Chenal et al., 2022). In climate model simulations, the historical warming patterns are close to the 1pctCO<sub>2</sub> patterns and both are different from the observed warming patterns meaning the quantitative impact of the pattern effect on historical warming is likely different to the results shown in this study. Nonetheless, our analysis highlight that the forced pattern effect could be responsible for about 10% of the global surface warming regardless of the geometry of the patterns suggesting that in the historical period the pattern effect also affected the historical GMST. Further study is required to quantify how the historical pattern actually affected the historical GMST and also how such an historical pattern would affect decadal climate projections if it was forced and thus persistent over the decades to come (Alessi & Rugenstein, 2023). These could be conducted using the framework we introduce here on quantifying the impact of the pattern effect on GMST change

## Conclusion

In this paper, we have quantified the pattern effect in 1pctCO<sub>2</sub> experiments and determine its influence on decadal global warming. To do so, we separated the radiative response induced by uniform warming from the radiative response induced by changing warming patterns. Overall, we found that the pattern effect is essentially forced and is negative in 1pctCO<sub>2</sub> experiments, which consequently dampens global warming. Notably, we show that the transient climate response is reduced by 11% on average because of the pattern effect. We also found differences in climate models, and highlighted that the forced pattern effect can significantly affect decadal warming. Our results are representative of the forced pattern effect in historical simulations but further work is required to determine the influence of other forcing agents, such as aerosols, and of the modes of atmosphere-ocean internal variability on global warming through the pattern effect. We highlight that the impact on the GMST of high frequency variability of the pattern effect, such as associated with ENSO, should be largely attenuated, while the PDO may substantially influence decadal warming.

We acknowledge the World Climate Research Programme’s Working Group on Coupled Modelling, which is responsible for CMIP, and we thank the climate modelling groups for producing and making available their model output, specifically modelling groups participating in CFMIP and RFMIP. We also thank Yue Dong, Chen Zhou and Bosong Zhang for making their Green’s functions outputs available online. The authors declare no conflict of interest.

CMIP data used in this study are available on the Earth System Grid Foundation, at <https://esgf.llnl.gov/>. CAM4 Green’s functions are available on Yue Dong’s personal website at <https://sites.google.com/view/yuedong-atmos/data>. CAM5 Green’s functions are available at <https://github.com/mzelinka/greens-function>. GFDL-CM4 were provided by Bosong Zhang. Scripts for the processing and figures in this paper will be made available as a zenodo archive.

Mode parameters for the two layer ocean model Following (Geoffroy et al., 2013; Rohrschneider et al., 2019), using the two layer ocean model to represent the ocean inertia yields the following GMST change in response to the change in radiative forcing  $F$  and to the pattern  $P$  (Equation 6):

$$\left\{ \begin{aligned} \bar{T}_F(t) &= \frac{1}{C(\psi_s + \psi_f)} \left( \psi_f \int_0^t F(s) e^{-\frac{t-s}{\tau_f}} ds + \psi_s \int_0^t F(s) e^{-\frac{t-s}{\tau_s}} ds \right) \\ \bar{T}_P(t) &= \frac{1}{C(\psi_s + \psi_f)} \left( \psi_f \int_0^t P(s) e^{-\frac{t-s}{\tau_f}} ds + \psi_s \int_0^t P(s) e^{-\frac{t-s}{\tau_s}} ds \right) \end{aligned} \right.$$

(17)

Where  $\tau_s$  and  $\tau_f$  are slow and fast characteristic timescales respectively and  $\psi_s$  and  $\psi_f$  are mode parameters. These four parameters can be obtained by combining the ocean model parameters  $C$ ,  $C_0$  and  $\gamma$  with the uniform warming climate feedback parameter  $\lambda_u$  with:

$$\left\{ \begin{aligned} b &= \frac{\lambda_u + \gamma}{C} + \frac{\gamma}{C_0} & b^* &= \frac{\lambda_u + \gamma}{C} - \frac{\gamma}{C_0} & \delta &= b^2 - 4 \frac{\lambda_u \gamma}{CC_0} \\ \tau_f &= \frac{CC_0}{2\lambda_u \gamma} (b - \sqrt{\delta}) & \tau_s &= \frac{CC_0}{2\lambda_u \gamma} (b + \sqrt{\delta}) \\ \psi_f &= \frac{C}{2\gamma} (b^* - \sqrt{\delta}) & \psi_s &= \frac{C}{2\gamma} (b^* + \sqrt{\delta}) \end{aligned} \right.$$

(18)

More details on how to determine these parameters are provided in (Geoffroy et al., 2013; Rohrschneider et al., 2019).

## References

- Developing climate scenarios from equilibrium GCM results.* (1990).
- Pattern scaling: an examination of the accuracy of the technique for describing future climates. (2003). *Climatic Change*, 60(3), 217–242.
- A scaling approach to project regional sea level rise and its uncertainties. (2013). *Earth System Dynamics*, 4(1), 11–29.
- Limits to global and Australian temperature change this century based on expert judgment of climate sensitivity. (2017). *Climate Dynamics*, 48, 3325–3339.
- The Warming Papers: The Scientific Foundation for the Climate Change Forecast.* (2011). John Wiley & Sons.
- The Dependence of Radiative Forcing and Feedback on Evolving Patterns of Surface Temperature Change in Climate Models. (2015). *Journal of Climate*, 28(4), 1630–1648. <https://doi.org/10.1175/JCLI-D-14-00545.1>
- Time-Varying Climate Sensitivity from Regional Feedbacks. (2013). *Journal of Climate*, 26(13), 4518–4534. <https://doi.org/10.1175/JCLI-D-12-00544.1>
- Prospects for Narrowing Bounds on Earth’s Equilibrium Climate Sensitivity. (2016). *Earth’s Future*, 4(11), 512–522. <https://doi.org/10.1002/2016EF000376>
- Chapter 7: The Earth’s Energy Budget, Climate Feedbacks and Climate Sensitivity. (2021). *The Earth*, 132. <https://doi.org/10.1017/9781009157896.009>
- The Dependence of Global Cloud and Lapse Rate Feedbacks on the Spatial Structure of Tropical Pacific Warming. (2018). *Journal of Climate*, 31(2), 641–654. <https://doi.org/10.1175/JCLI-D-17-0087.1>
- Relationship of Tropospheric Stability to Climate Sensitivity and Earth’s Observed Radiation Budget. (2017). *Proceedings of the National Academy of Sciences*, 114(50), 13126–13131. <https://doi.org/10.1073/pnas.1714308114>
- Model Spread in Tropical Low Cloud Feedback Tied to Overturning Circulation Response to Warming. (2022). *Nature Communications*, 13(1), 7119. <https://doi.org/10.1038/s41467-022-34787-4>
- Analyzing the Dependence of Global Cloud Feedback on the Spatial Pattern of Sea Surface Temperature Change with a Green’s Function Approach. (2017). *Journal of Advances in Modeling Earth Systems*, 9(5), 2174–2189. <https://doi.org/10.1002/2017MS001096>
- Accounting for Changing Temperature Patterns Increases Historical Estimates of Climate Sensitivity. (2018). *Geophysical Research Letters*, 45(16), 8490–8499.
- On the Effect of Historical SST Patterns on Radiative Feedback. (2022). *Journal of Geophysical Research: Atmospheres*, 127(18), e2022JD036675. <https://doi.org/10.1029/2022JD036675>
- Energy Budget Constraints on Climate Sensitivity in Light of Inconstant Climate Feedbacks. (2017). *Nature Climate Change*, 7(5), 331–335. <https://doi.org/10.1038/nclimate3278>
- Biased Estimates of Equilibrium Climate Sensitivity and Transient Climate Response Derived from Historical CMIP6 Simulations. (2021). *Geophysical Research Letters*, 48(24), e2021GL095778.
- Internal Variability and Disequilibrium Confound Estimates of Climate Sensitivity from Observations. (2018). *Geophysical Research Letters*, 45(3), 1595–1601.
- An Assessment of Earth’s Climate Sensitivity Using Multiple Lines of Evidence. (2020). *Reviews of Geophysics*, 58(4), e2019RG000678. <https://doi.org/10.1029/2019RG000678>

Greater Committed Warming after Accounting for the Pattern Effect. (2021). *Nature Climate Change*, 1–5. <https://doi.org/10.1038/s41558-020-00955-x>

Antarctic Ice-Sheet Meltwater Reduces Transient Warming and Climate Sensitivity Through the Sea-Surface Temperature Pattern Effect. (2022). *Geophysical Research Letters*, 49(24), e2022GL101249. <https://doi.org/10.1029/2022GL101249>

Do Southern Ocean Cloud Feedbacks Matter for 21st Century Warming?. (2017). *Geophysical Research Letters*, 44(24), 12,447–412,456. <https://doi.org/10.1002/2017GL076339>

Surface Temperature Pattern Scenarios Suggest Higher Warming Rates Than Current Projections. (2023). *Geophysical Research Letters*, 50(23), e2023GL105795. <https://doi.org/10.1029/2023GL105795>

Revisiting the Global Energy Budget Dynamics with a Multivariate Earth Energy Balance Model to Account for the Warming Pattern Effect. (2023). *Journal of Climate*, -1(aop). <https://doi.org/10.1175/JCLI-D-22-0765.1>

The Effect of Solar Radiation Variations on the Climate of the Earth. (1969). *Tellus*, 21(5), 611–619.

A Global Climatic Model Based on the Energy Balance of the Earth-Atmosphere System. (1969). *Journal of Applied Meteorology*, 8(3), 392–400. [https://doi.org/10.1175/1520-0450\(1969\)008<0392:AGCMB0>2.0.CO;2](https://doi.org/10.1175/1520-0450(1969)008<0392:AGCMB0>2.0.CO;2)

*Energy Balance Climate Models*. (2017). John Wiley & Sons.

Attributing Historical and Future Evolution of Radiative Feedbacks to Regional Warming Patterns Using a Green’s Function Approach: The Preeminence of the Western Pacific. (2019). *Journal of Climate*, 32(17), 5471–5491. <https://doi.org/10.1175/JCLI-D-18-0843.1>

Slow Modes of Global Temperature Variability and Their Impact on Climate Sensitivity Estimates. (2021). *Journal of Climate*, 34(21), 8717–8738. <https://doi.org/10.1175/JCLI-D-20-1013.1>

Time-Variations of the Climate Feedback Parameter Are Associated with the Pacific Decadal Oscillation. (2023). *Communications Earth & Environment*, 4(1), 1–10. <https://doi.org/10.1038/s43247-023-00887-2>

Using a Green’s Function Approach to Diagnose the Pattern Effect in GFDL AM4 and CM4. (2023). *Journal of Climate*, 36(4), 1105–1124. <https://doi.org/10.1175/JCLI-D-22-0024.1>

The Green’s Function Model Intercomparison Project (GFMIIP) Protocol. (2024). *Journal of Advances in Modeling Earth Systems*, 16(2), e2023MS003700. <https://doi.org/10.1029/2023MS003700>

A Refined Model for the Earth’s Global Energy Balance. (2019). *Climate Dynamics*, 53(7-8), 4781–4797. <https://doi.org/10.1007/s00382-019-04825-x>

Observational Evidence for Two Modes of Coupling between Sea Surface Temperatures, Tropospheric Temperature Profile, and Shortwave Cloud Radiative Effect in the Tropics. (2019). *Geophysical Research Letters*, 46(16), 9890–9898. <https://doi.org/10.1029/2019GL083990>

Convergence Rate and Stability of Ocean-Atmosphere Coupling Schemes with a Zero-Dimensional Climate Model. (1981). *Journal of Atmospheric Sciences*, 38(10), 2112–2120.

Vertical Heat Transports in the Ocean and Their Effect on Time-Dependent Climate Change. (2000). *Climate Dynamics*, 16(7), 501–515.

The Role of Climate Sensitivity and Ocean Heat Uptake on AOGCM Transient Temperature Response. (2002). *Journal of Climate*, 15(1), 124–130. [https://doi.org/10.1175/1520-0442\(2002\)015<0124:TROCSA>2.0.CO;2](https://doi.org/10.1175/1520-0442(2002)015<0124:TROCSA>2.0.CO;2)

- Probing the Fast and Slow Components of Global Warming by Returning Abruptly to Preindustrial Forcing. (2010). *Journal of Climate*, 23(9), 2418–2427. <https://doi.org/10.1175/2009JCLI3466.1>
- Transient Climate Response in a Two-Layer Energy-Balance Model. Part I : Analytical Solution and Parameter Calibration Using CMIP5 AOGCM Experiments. (2013). *Journal of Climate*, 26(6), 1841–1857.
- On Simple Representations of the Climate Response to External Radiative Forcing. (2019). *Climate Dynamics*, 53(5), 3131–3145. <https://doi.org/10.1007/s00382-019-04686-4>
- Masson-Delmotte, V., Zhai, P., Pirani, A., Connors, S. L., Péan, C., Berger, S., Caud, N., Chen, Y., Goldfarb, L., Gomis, M. I., Huang, M., Leitzell, K., Lonnoy, E., Matthews, J. B. R., Maycock, T. K., Waterfield, T., Yelekçi, O., Yu, R., & Zhou, B. (Eds.). (2021). The Earth’s Energy Budget, Climate Feedbacks, and Climate Sensitivity Supplementary Material [Book Section]. In *Climate Change 2021: The Physical Science Basis. Contribution of Working Group I to the Sixth Assessment Report of the Intergovernmental Panel on Climate Change*. Cambridge University Press.
- Overview of the Coupled Model Intercomparison Project Phase 6 (CMIP6) Experimental Design and Organization. (2016). *Geoscientific Model Development*, 9(5), 1937–1958.
- What Climate Sensitivity Index Is Most Useful for Projections?. (2018). *Geophysical Research Letters*, 45(3), 1559–1566. <https://doi.org/10.1002/2017GL075742>
- The Cloud Feedback Model Intercomparison Project (CFMIP) Contribution to CMIP6. (2017). *Geoscientific Model Development*, 10(1), 359–384. <https://doi.org/10.5194/gmd-10-359-2017>
- The Beijing Climate Center Climate System Model (BCC-CSM): The Main Progress from CMIP5 to CMIP6. (2019). *Geoscientific Model Development*, 12(4), 1573–1600. <https://doi.org/10.5194/gmd-12-1573-2019>
- The Community Earth System Model Version 2 (CESM2). (2020). *Journal of Advances in Modeling Earth Systems*, 12(2), e2019MS001916. <https://doi.org/10.1029/2019MS001916>
- Evaluation of CMIP6 Deck Experiments with CNRM-CM6-1. (2019). *Journal of Advances in Modeling Earth Systems*, 11(7), 2177–2213. <https://doi.org/10.1029/2019MS001683>
- The Canadian Earth System Model Version 5 (CanESM5. 0.3). (2019). *Geoscientific Model Development*, 12(11), 4823–4873.
- Energy Exascale Earth System Model v1.0*. (2018).
- The GFDL Earth System Model Version 4.1 (GFDL-ESM 4.1): Overall Coupled Model Description and Simulation Characteristics. (2020). *Journal of Advances in Modeling Earth Systems*, 12(11), e2019MS002015. <https://doi.org/10.1029/2019MS002015>
- GISS-E2.1: Configurations and Climatology. (2020). *Journal of Advances in Modeling Earth Systems*, 12(8), e2019MS002025. <https://doi.org/10.1029/2019MS002025>
- The Met Office Global Coupled Model 3.0 and 3.1 (GC3.0 and GC3.1) Configurations. (2018). *Journal of Advances in Modeling Earth Systems*, 10(2), 357–380. <https://doi.org/10.1002/2017MS001115>
- Presentation and Evaluation of the IPSL-CM6A-LR Climate Model. (2020). *Journal of Advances in Modeling Earth Systems*, 12(7), e2019MS002010.
- Description and Basic Evaluation of Simulated Mean State, Internal Variability, and Climate Sensitivity in MIROC6. (2019). *Geoscientific Model Development*, 12(7), 2727–2765.
- The Meteorological Research Institute Earth System Model Version 2.0, MRI-ESM2. 0: Description and Basic Evaluation of the Physical Component. (2019). *Journal of the Meteorological Society of Japan. Ser. II*, 97(5), 931–965.

Overview of the Norwegian Earth System Model (NorESM2) and Key Climate Response of CMIP6 DECK, Historical, and Scenario Simulations. (2020). *Geoscientific Model Development*, 13(12), 6165–6200.

The Mean Climate of the Community Atmosphere Model (CAM4) in Forced SST and Fully Coupled Experiments. (2013). *Journal of Climate*, 26(14), 5150–5168. <https://doi.org/10.1175/JCLI-D-12-00236.1>

Description of the NCAR Community Atmosphere Model (CAM 5.0). (2010). *NCAR Tech. Note NCAR/TN-486+ STR*, 1(1), 1–12.

The GFDL Global Atmosphere and Land Model AM4.0/LM4.0: 2. Model Description, Sensitivity Studies, and Tuning Strategies. (2018). *Journal of Advances in Modeling Earth Systems*, 10(3), 735–769. <https://doi.org/10.1002/2017MS001209>

Intercomparison and Interpretation of Climate Feedback Processes in 19 Atmospheric General Circulation Models. (1990). *Journal of Geophysical Research: Atmospheres*, 95(D10), 16601–16615.

A New Conceptual Model of Global Ocean Heat Uptake. (2023). *Climate Dynamics*. <https://doi.org/10.1007/s00382-023-06989-z>

An Energy Budget Framework to Understand Mechanisms of Land–Ocean Warming Contrast Induced by Increasing Greenhouse Gases. Part I: Near-Equilibrium State. (2021). *Journal of Climate*, 34(23), 9279–9292. <https://doi.org/10.1175/JCLI-D-21-0302.1>

Global and Regional Climate Feedbacks in Response to Uniform Warming and Cooling. (2023). *Journal of Geophysical Research: Atmospheres*, 128(24), e2023JD038861. <https://doi.org/10.1029/2023JD038861>

Global Atmospheric Sensitivity to Tropical SST Anomalies throughout the Indo-Pacific Basin. (2002). *Journal of Climate*, 15(23), 3427–3442.

Explaining Forcing Efficacy With Pattern Effect and State Dependence. (2023). *Geophysical Research Letters*, 50(3), e2022GL101700. <https://doi.org/10.1029/2022GL101700>

Circus Tents, Convective Thresholds, and the Non-Linear Climate Response to Tropical SSTs. (2023). *Geophysical Research Letters*, 50(6), e2022GL101499. <https://doi.org/10.1029/2022GL101499>

New Estimates of Radiative Forcing Due to Well Mixed Greenhouse Gases. (1998). *Geophysical Research Letters*, 25(14), 2715–2718. <https://doi.org/10.1029/98GL01908>

Why the Forcing from Carbon Dioxide Scales as the Logarithm of Its Concentration. (2022). *Journal of Climate*, 35(13), 4027–4047. <https://doi.org/10.1175/JCLI-D-21-0275.1>

Efficacy of Climate Forcings. (2005). *Journal of Geophysical Research: Atmospheres*, 110(D18). <https://doi.org/10.1029/2005JD005776>

The Radiative Forcing Model Intercomparison Project (RFMIP): Experimental Protocol for CMIP6. (2016). *Geoscientific Model Development (Online)*, 9(9).

Recommendations for Diagnosing Effective Radiative Forcing from Climate Models for CMIP6. (2016). *Journal of Geophysical Research: Atmospheres*, 121(20), 12,460–412,475. <https://doi.org/10.1002/2016JD025320>

Understanding Rapid Adjustments to Diverse Forcing Agents. (2018). *Geophysical Research Letters*, 45(21), 12,023–012,031. <https://doi.org/10.1029/2018GL079826>

An Ensemble of AMIP Simulations with Prescribed Land Surface Temperatures. (2018). *Geoscientific Model Development*, 11(9), 3865–3881.

Effective Radiative Forcing in a GCM With Fixed Surface Temperatures. (2021). *Journal of Geophysical Research: Atmospheres*, 126(4), e2020JD033880. <https://doi.org/10.1029/2020JD033880>

The El Niño–Southern Oscillation Pattern Effect. (2021). *Geophysical Research Letters*, 48(21), e2021GL095261. <https://doi.org/10.1029/2021GL095261>

Interdecadal Variations of Radiative Feedbacks Associated With the El Niño and Southern Oscillation (ENSO) in CMIP6 Models. (2023). *Geophysical Research Letters*, 50(23), e2023GL106127. <https://doi.org/10.1029/2023GL106127>

Potential Problems Measuring Climate Sensitivity from the Historical Record. (2020). *Journal of Climate*, 33(6), 2237–2248.

Changes in Earth’s Energy Budget during and after the “Pause” in Global Warming: An Observational Perspective. (2018). *Climate*, 6(3), 62.

The Inconstancy of the Transient Climate Response Parameter under Increasing CO<sub>2</sub>. (2015). *Philosophical Transactions of the Royal Society A: Mathematical, Physical and Engineering Sciences*, 373(2054), 20140417. <https://doi.org/10.1098/rsta.2014.0417>

Radiative Forcing of Carbon Dioxide, Methane, and Nitrous Oxide: A Significant Revision of the Methane Radiative Forcing. (2016). *Geophysical Research Letters*, 43(24), 12,614–612,623. <https://doi.org/10.1002/2016GL071930>

Climate Sensitivity Increases Under Higher CO<sub>2</sub> Levels Due to Feedback Temperature Dependence. (2021). *Geophysical Research Letters*, 48(4). <https://doi.org/10.1029/2020GL089074>

Impacts of the Unforced Pattern Effect on the Cloud Feedback in CERES Observations and Climate Models. (2022). *Geophysical Research Letters*, 49(2). <https://doi.org/10.1029/2021GL096299>

Time-Evolving Radiative Feedbacks in the Historical Period. (2023). *Journal of Geophysical Research: Atmospheres*, 128(20), e2023JD038984. <https://doi.org/10.1029/2023JD038984>

Contribution of Anthropogenic Aerosols to Persistent La Niña-like Conditions in the Early 21st Century. (2024). *Proceedings of the National Academy of Sciences*, 121(5), e2315124121. <https://doi.org/10.1073/pnas.2315124121>

Aerosols Hold the Key to Recent and Future Pacific Warming Patterns. (2024). *Proceedings of the National Academy of Sciences*, 121(6), e2322594121. <https://doi.org/10.1073/pnas.2322594121>

Climate Feedback to Stratospheric Aerosol Forcing: The Key Role of the Pattern Effect. (2022). *Journal of Climate*, 35(24), 7903–7917.

Persistent Discrepancies between Observed and Modeled Trends in the Tropical Pacific Ocean. (2022). *Journal of Climate*, 35(14), 4571–4584. <https://doi.org/10.1175/JCLI-D-21-0648.1>

Systematic Climate Model Biases in the Large-Scale Patterns of Recent Sea-Surface Temperature and Sea-Level Pressure Change. (2022). *Geophysical Research Letters*, 49(17), e2022GL100011. <https://doi.org/10.1029/2022GL100011>

The Peculiar Trajectory of Global Warming. (2021). *Journal of Geophysical Research: Atmospheres*, 126(4), e2020JD033629.

Observational Constraint on the Climate Sensitivity to Atmospheric CO<sub>2</sub> Concentrations Changes Derived from the 1971–2017 Global Energy Budget. (2022). *Journal of Climate*, 35(14), 4469–4483.